Electronic Supplementary Material (ESI) for Nanoscale Horizons.
This journal is © The Royal Society of Chemistry 2019

Supporting Information

Single-layer boron-doped graphene quantum dots for contrast-enhanced in vivo T1-weighted MRI

Hui Wang, [a,b‡] *Richard Revia,*[a‡] *Qingxin Mu,*[a] *Guanyou Lin,*[a] *Charles Yen*[a] *and Miqin Zhang*[a*]

[a] Department of Materials Science and Engineering, University of Washington, Seattle, Washington 98195, United States. E-mail: mzhang@uw.edu

[b] The Anhui Key Laboratory of Condensed Matter Physics at Extreme Conditions, High Magnetic Field Laboratory, Hefei Institutes of Physical Science, Chinese Academy of Sciences, Hefei, Anhui 230031, China.

‡These authors contributed equally to this work.

Experimental Section

Synthesis of single-layer boron-doped graphene quantum dots (SL-BGQDs): All chemicals were purchased from Sigma-Aldrich (St. Louis, MO, USA). VPBA (0.05 g) and boric acid (0.03 g) were dissolved in a solution of 20 mL acetone and 5 mL ethanol. After intense sonication for 30 min, 10.0 mL of H_2O_2 (30%) was slowly added to the solution. The solution was then ultrasonicated for 10 min and transferred into a 50 mL Teflon-lined, stainless-steel autoclave. This precursor solution was heated to and maintained at 205°C. After 24 h, the solution was cooled naturally to room temperature. The resultant solution was dialyzed for 3 days (Spectra/Per molecular porous membrane tubing, cutoff 14 kDa) at room temperature. The aqueous dispersion of SL-BGQDs was then collected and centrifuged at 14,800 rpm for 30 min with the supernatant discarded.

Characterization: Transmission electron microscopy (TEM) and high-resolution TEM (HRTEM) images were acquired on a Tecnai G2 F20 electron microscope (FEI, Hillsboro, OR) operating at a voltage of 200 kV. Atomic force microscopy (AFM) was performed using a Veeco DI Nano-scope MultiMode V system. Powder X-ray diffraction (XRD) patterns were acquired from lyophilized samples using a D8 Bruker X-ray diffractometer with Cu Kα radiation. UV-vis absorption spectra were obtained on a UV-vis Spectrometer (Agilent Technologies, Santa Clara, CA). Magnetic properties were measured using a superconducting quantum interference device magnetometer (Quantum Design MPMS XL-7). The sample preparation process was performed using a non-metallic container. Fourier transform infrared (FTIR) spectra were acquired using a Nicolet 5-DXB FTIR spectrometer with a resolution of 4 cm^{-1}. Raman spectra were taken on a Raman-Microscope (Renishaw-InVia) using a 514.5 nm Ar^+ laser at room temperature. Photoluminescence (PL) spectra were obtained on a JOBIN YVON Co. FluoroMax®-3 spectrofluorometer equipped with a Hamamatsu R928P

photomultiplier tube. X-ray photoelectron spectroscopy (XPS) experiments were conducted at the National ESCA and Surface Analysis Center at the University of Washington.

Penetration of the blood-brain barrier by SL-BGQDs: All procedures involving animals were performed in accordance with University of Washington Institutional Animal Care and Use Committee regulations. C57BL/6 wild-type mice (Charles River Laboratories, Inc.) were euthanized 1 h post tail-vein injection with SL-BGQDs (dispersed in PBS, 200 μL, 1 mg mL^{-1}) or PBS (200 μL, control), and brain tissues were dissected. The tissues were preserved in 10% formalin for 48 h. Formalin-fixed tissue samples were first transferred from PBS to and maintained for 2 h in 70% ethanol and were then transferred into and maintained for an additional 2 h in 95% ethanol/5% methanol. The samples were then transferred to and maintained for 1 h in absolute ethanol and then transferred again into and maintained in 3 consecutive absolute xylene solutions, each for 1 h. After dehydration, the samples were placed consecutively in 2 melted paraffin baths, each for 2 h. The paraffin-penetrated samples were embedded in paraffin blocks, sectioned at 10 μm thickness and loaded onto microscope slides. The loaded slides were first heated to remove excess paraffin, and the samples were adhered to the slides. Subsequently, the samples were deparaffinized by a series of xylene, ethanol, and PBS baths. The slides were then rinsed and stained with DAPI and anti-CD31 antibody for 15 min at room temperature. Coverslips were then mounted onto microscope slides using Prolong Gold Antifade Mountant. Images were acquired on a Leica SP8X confocal laser scanning microscope.

Viability of cells treated with SL-BGQDs or Gd-DTPA: 4T1, SF763, and B16F10 cells were seeded in 96-well plates and incubated overnight in Dulbecco's Modified Eagle Medium (DMEM). On the following day, the medium was replaced with a medium containing SL-BGQDs or Gd-DTPA, or with PBS (control). Three concentrations of SL-BGQDs or Gd-

DTPA (200, 150, and 100 μg mL^{-1}) were used, and samples at each concentration were ran in sextuplicate. Cells were incubated with SL-BGQDs, Gd-DTPA, or PBS for 72 h. Cell viability was assessed using the Alamar Blue assay. Briefly, the medium was replaced with a cell culture medium containing the Alamar Blue reagent and incubated for 2 h. Following the incubation, a microplate reader (SpectraMax i3, Molecular Devices, Sunnyvale, CA) was used to determine the fluorescence intensity of SL-BGQDs or Gd-DTPA. The fluorescence intensity from SL-BGQD or Gd-DTPA treated cells was normalized to the intensity from PBS-treated control cells to determine percent viability.

Histopathological evaluation and nucleus morphology evaluation of organs from mice treated with SL-BGQDs or Gd-DTPA: Five days after receiving no injection (control) or tail vein injection of SL-BGQD or Gd-DTPA at a concentration of 5 mg mL^{-1} (dispersed in PBS), the C57BL/6 wild-type mice (Charles River Laboratories, Inc.) were euthanized and whole organs (kidneys, liver, lung, and spleen) were removed and preserved in 10% formalin for 48 h. The tissues were then embedded in paraffin, sliced into 5 μm sections, and stained with hematoxylin and eosin (H&E). Microscopic images of the tissues were acquired using a Nikon ECLIPSE TE2000-S microscope.

Tissue slide samples were prepared in a similar fashion as those for H&E staining. The samples were deparaffinized and then processed with DAPI staining. The samples were then viewed under a microscope to identify any abnormal nucleus morphology.

Hematology assay: Twenty-four hours after mice were tail-vein injected with SL-BGQDs or Gd-DTPA at a concentration of 5 mg mL^{-1} (dispersed in PBS), 3mL of blood was drawn from C57BL/6 wild-type mice (n = 4) using the cardiac puncture method after terminal deep anesthesia. Animals receiving PBS injection (n = 4) were used as controls. Collected samples

were sent to the Laboratory Medicine Research Testing Service at the University of Washington for chemical and phlebotomy analyses.

RT-PCR assay: 24 h after mice were tail-vein injected with SL-BGQDs or Gd-DTPA at a concentration of 5 mg mL^{-1} (dispersed in PBS), 20 mg of each harvested tissue from each contrast agent-treated mouse was flash-frozen using liquid nitrogen and grounded into a fine powder. The powder was then transferred into a microfuge tube and treated with RNeasy Plus Mini kit (Qiagen, Germany) for the extraction of mRNA. RT-PCR was carried out following the mRNA extraction process using the following primer sets:

Target genes	forward primer	reverse primer
xbp-1s	5'-TGCTGAGTCCGCAGCAGGTG-3'	5'-GACTAGCAGACTCTGGGGAAGG-3'
chop	5'-CATACACCACCACACCTGAAAG-3'	5'-CCGTTTCCTAGTTCTTCCTTGC-3'
bip	5'-GAAAGGATGGTTATGATGCTGAG-3'	5'-GTCTTCAATGTCCGCATCCTG-3'
IL-1β	5'-ATGGCAACTGTTCCTGAACTCAAC-3'	5'-CAGGACAGGTATAGATTCTTTCC-3'
TNF-α	5'-ACGTGGAACTGGCAGAAGAG-3'	5'-CTCCTCCACTTGGTGGTTTG-3'
Gapdh	5'-GACTTCAACAGCAACTCCCAC-3'	5'-TCCACCACCCTGTTGCTGTA-3'

The expression of genes was then quantified relative to the expression level of *Gapdh*.

In vitro MR imaging: T_1- and T_2-weighted imaging and quantitative T_1 and T_2 MR imaging scan sequences were used to investigate the contrast enhancing capabilities of SL-BGQDs. MR imaging was performed on a Bruker Avance III 600 MHz, 14 T wide bore spectrometer. Either SL-BGQDs or Gd-DTPA samples in PBS were pipetted into glass vials (3.25 mm I.D., 5 mm O.D., 200 μL volume). The vials were fixed in place inside a water reservoir; the water served as a homogeneous background signal to minimize magnetic susceptibility variations near samples. The secured vials were placed in a 25 mm single-channel ^{1}H radiofrequency receiving coil (PB Micro 2.5). Relaxation properties of SL-BGQDs and Gd-DTPA were

evaluated with a quantitative T_1 rapid imaging with refocused echoes and variable repetition time (RARE-VTR) pulse sequence with an echo time (TE) of 12.0 ms; TR = 80 ms, 400 ms, 800 ms, 1600 ms, 3000 ms, 6000 ms, 8000 ms, and 12000 ms; 180 × 180 μm^2 in-plane resolution; and 5.0 mm slice thickness for one slice. Quantitative T_2 values were measured using a multi-spin multi-echo (MSME) pulse sequence with TR = 2500 ms, TE = 6.7 + 6n ms (n = 0–16), and 78 × 156 μm^2 in-plane resolution with 0.5 mm slice thickness for 14 slices. T_1-weighted images were acquired with a RARE pulse sequence with TE = 5.49 ms, TR = 531 ms, 78 × 52 μm^2 in-plane resolution, and 0.5 mm slice thickness for 10 slices. T_2-weighted images were acquired with a RARE pulse sequence with TE = 6.78 ms, TR = 4000 ms, and 78 × 52 μm^2 in-plane resolution with 0.5 mm slice thickness for 14 slices. Analysis of MR imaging data was accomplished with the FMRIB software library (FSL), Paravision 5.1 analysis package (Bruker), and ImageJ (NIH). T_1 values were determined within a circular, 100-voxel region of interest.

In vivo MRI: 90 min sequential T_1-weighted imaging was performed over the abdominal regions of C57BL/6 wild-type mice before and after mice were injected with SL-BGQDs (200 μL, 1 mg mL^{-1}) or Gd-DTPA (200 μL, 1 mg mL^{-1}), using a Bruker Avance III 600 MHz, 14 T vertical-bore imaging system. Similarly, 10 min sequential T_1-weighted imaging was performed over the cranial regions of C57BL/6 wild-type mice before and after injection with SL-BGQDs (200 μL, 5 mg mL^{-1}) or Gd-DTPA (200 μL, 5 mg mL^{-1}). Mice were anesthetized with isoflurane (Piramal Healthcare) and secured in a coil-integrated respiratory monitoring system (SA Instruments; MR-compatible small animal monitoring and gating system) with nose-cone for oxygen/anesthetic, ear-bar head holder, circulating temperature control bath, and residual gas extraction. Abdominal scans were acquired using RARE T_1-weighted sequences (TR/TE = 691/5.5 ms, in-plane resolution 93 × 62 μm^2, matrix 256 × 284) with

slices placed in the transverse plane with 0.5 mm slice thickness and 0.75 mm interslice gaps allowing for coverage from the liver to the pelvic floor. Cranial scans were acquired over the entire head with a 3-dimensional, T_1-weighted fast low angle shot (FLASH) scan sequence (TR/TE = 16.2/2.7 ms, resolution 106 × 108 × 152 μm^3, matrix 284 × 186 × 132). Images presented resulting from this cranial scan sequence were processed using a maximum intensity projection with a 3 mm slab thickness.

Supplementary Figures

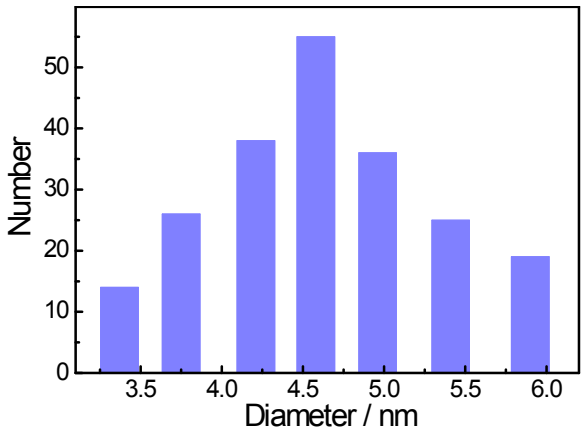

Figure S1. Size distribution of SL-BGQDs obtained by measuring approximately 200 particles from TEM images.

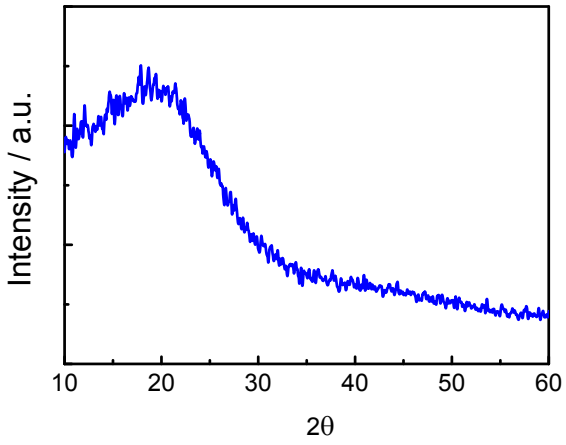

Figure S2. X-ray diffraction pattern of SL-BGQDs.

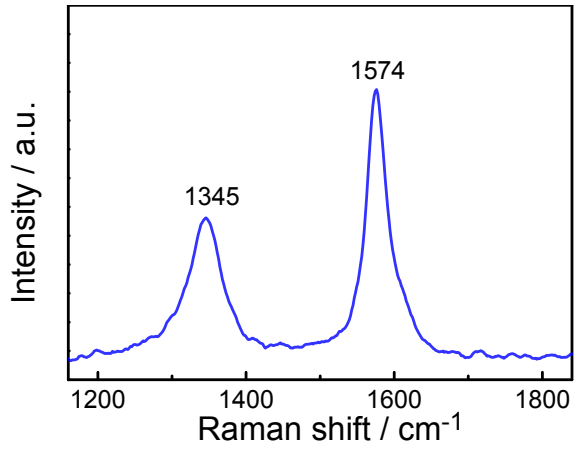

Figure S3. Raman spectrum of SL-BGQDs.

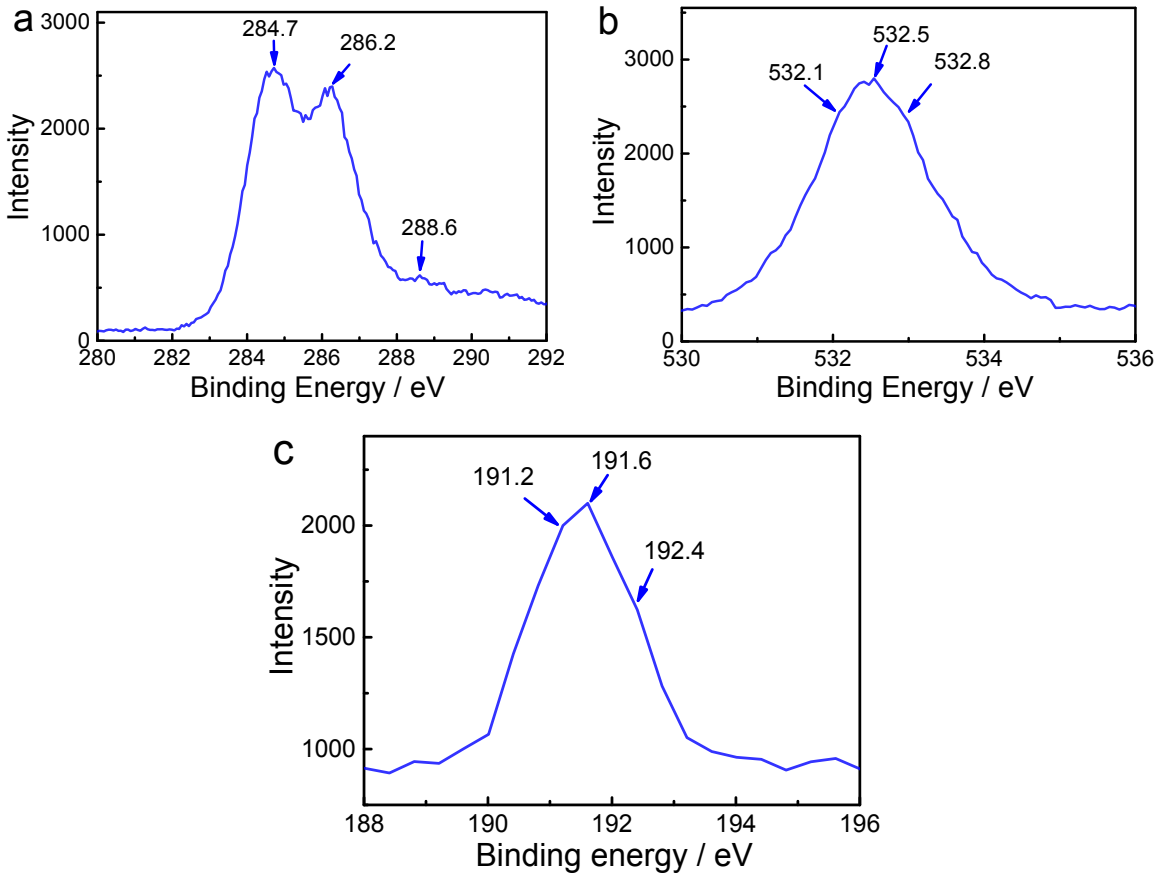

Figure S4. Surface properties of SL-BGQDs: XPS high-resolution survey scan of (a) C 1s. (b) O 1s and (c) B 1s. The C 1s peaks at 284.7, 286.2, and 288.6 eV are assigned to the carbon in forms of C−C (sp^3)/C=C (sp^2), C−O (sp^3), and O−C=O (sp^2), respectively.[1] The O 1s peaks at 532.1, 532.5, and 532.8 eV are associated with C=O quinone-type groups, C−OH phenol groups, and C−O−C ether groups, respectively.[2] The B 1s peaks at 191.2 and 191.6 eV are attributed to sp^2 C=B bonds.[3, 4] In addition, the B 1s peak at 192.4 eV is associated with B–O bonds.[5] The peaks at 191.2 and 191.6 eV further provide evidence of the boron doping in SL-BGQDs.

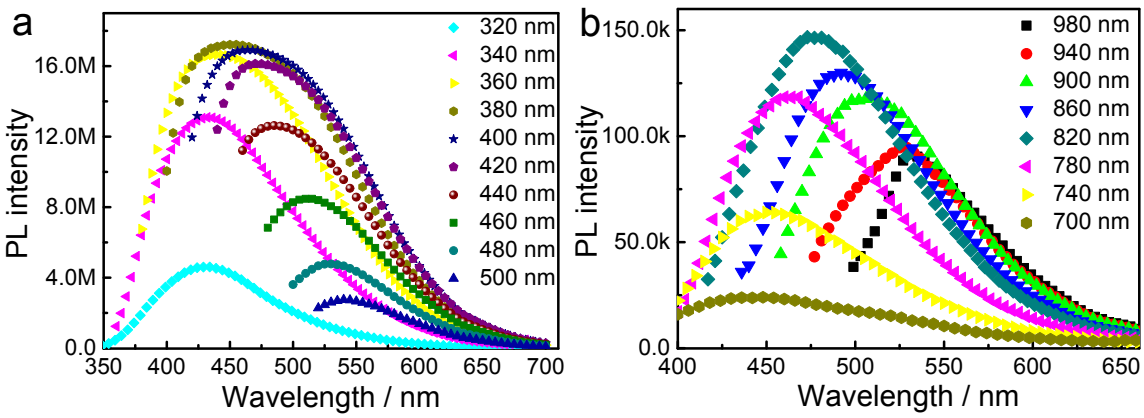

Figure S5. Photoluminescent properties of SL-BGQDs. (a) PL spectra and (b) upconverted PL spectra of SL-BGQDs under different excitation wavelengths from 320 nm 980 nm.

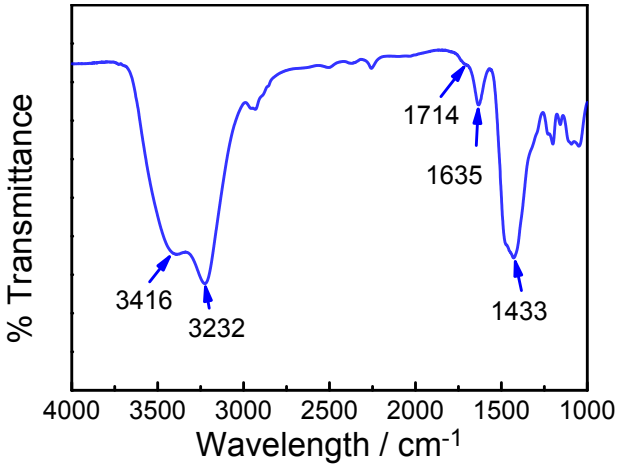

Figure S6. FT-IR spectrum of SL-BGQDs. An absorption peak of the O-H stretching at 3416 cm^{-1} and 3232 cm^{-1}, and the C=O stretching mode at 1714 cm^{-1}, corresponding to the carboxylic acid groups conjugated with condensed aromatic carbons.[6] A weak peak at 1383 cm^{-1} was attributed to the C-O vibration of a carboxylic acid group, and the C=C vibration of sp^2-hybridized carbon atoms was detected at 1600 cm^{-1}.

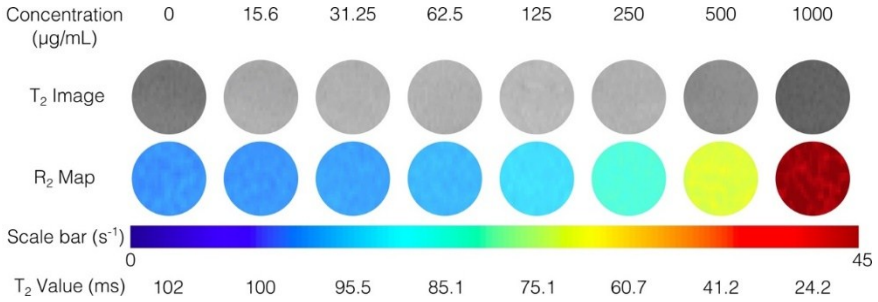

Figure S7. T_2-weighted MR images and R_2 maps of SL-BGQDs at different concentrations.

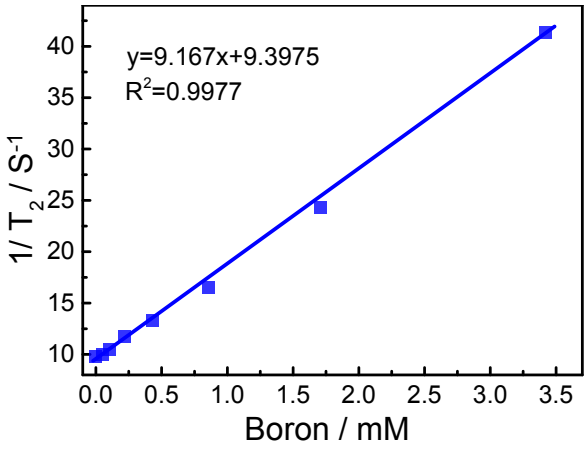

Figure S8. Plot of $1/T_2$ as a function of the boron concentration in SL-BGQDs. The slope of the curve is defined as the transverse relaxivity, r_2 (= 9.2 $mM^{-1}s^{-1}$).

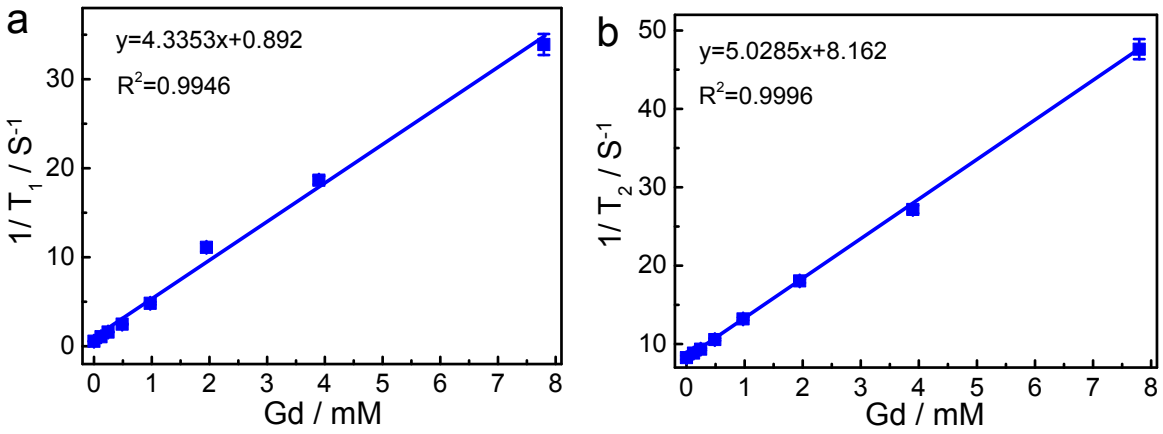

Figure S9. Plot of (a) $1/T_1$ and (b) $1/T_2$ as a function of Gd-DTPA concentration. The slopes are defined as the longitudinal relaxivity, r_1 (= 4.3 $mM^{-1}s^{-1}$) and the transverse relaxivity, r_2 (= 5.03 $mM^{-1}s^{-1}$), respectively.

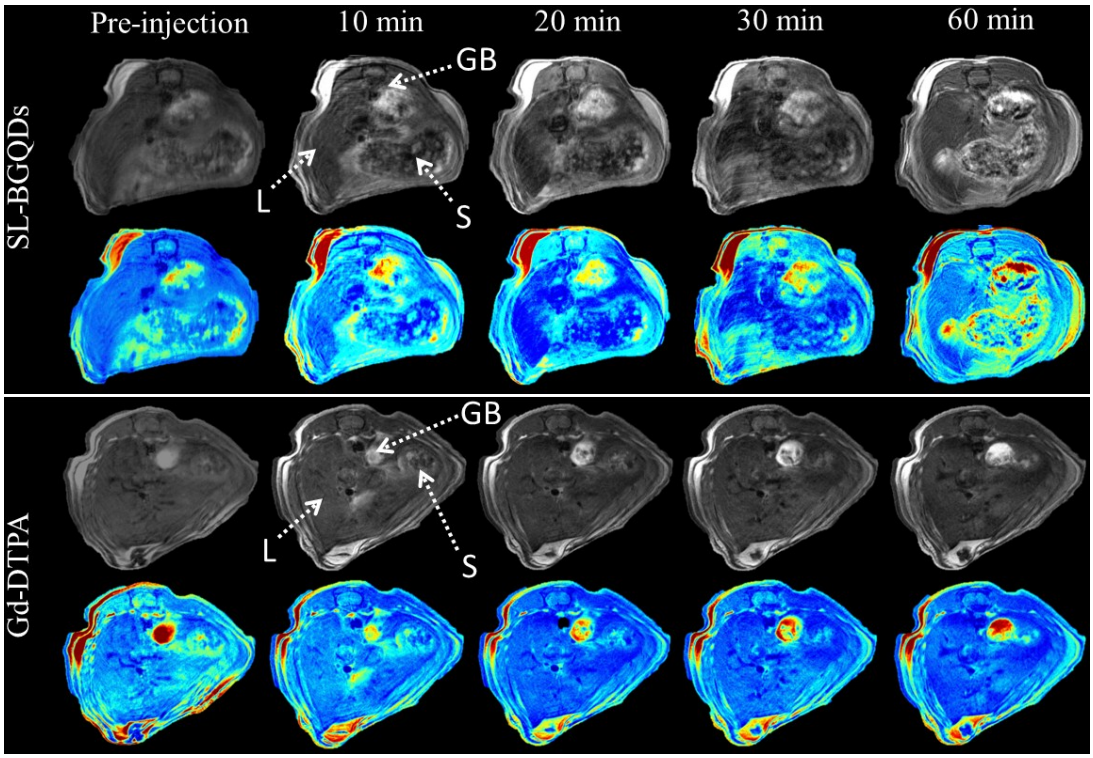

Figure S10. In vivo abdominal MR imaging. T_1-weighted MR images of the cross-sections of mice receiving SL-GQDs (top panel) and Gd-DTPA (bottom panel) treatments with dynamic time-resolved MR imaging acquired before and at various time points after intravenous contrast agent administration. Both grayscale and colorized images are displayed for each experimental group. The arrows denote various organs: liver (L), stomach (S), and gall bladder (GB).

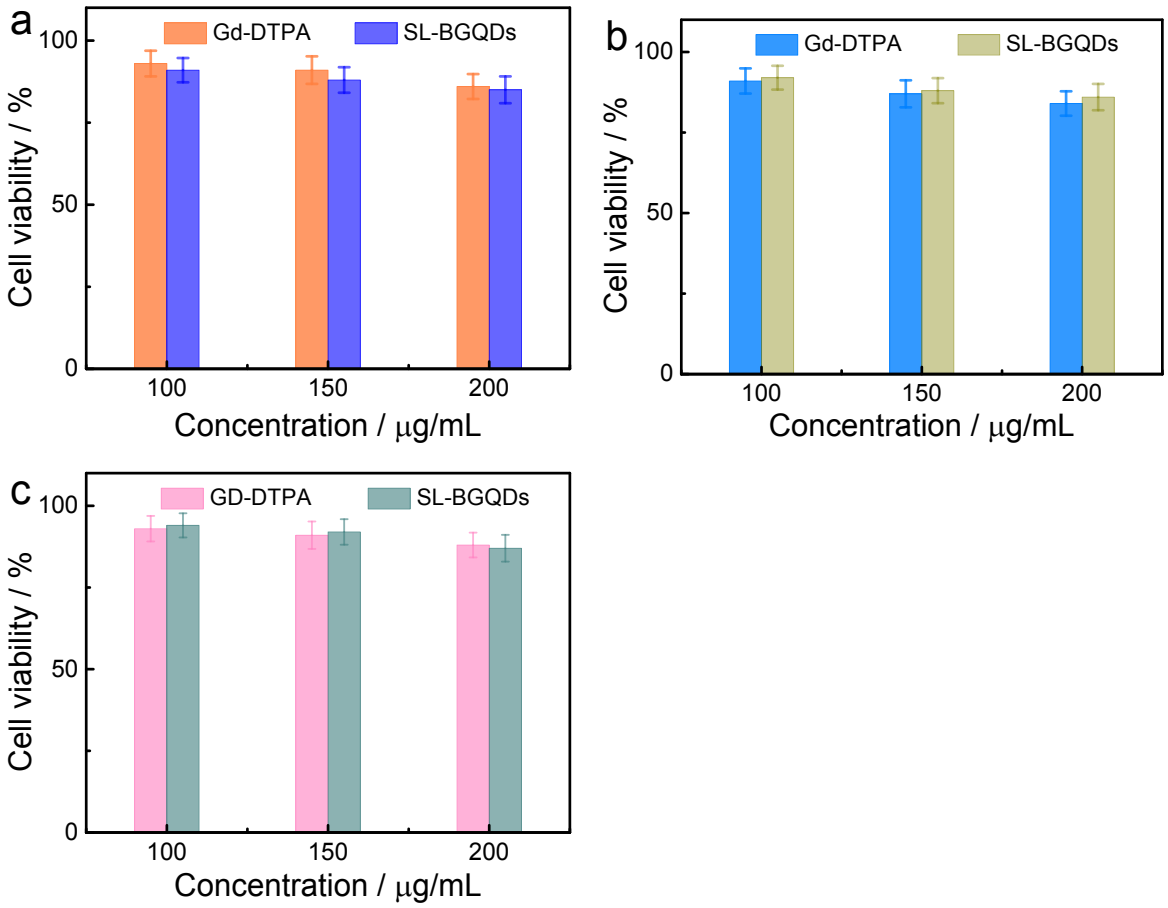

Figure S11. In vitro cytotoxicity study of SL-BGQDs and Gd-DTPA performed by assessing the viability of (a) 4T1, (b) SF763, and (c) B16F10 cell lines 72 h after treatment with SL-BGQDs or Gd-DTPA.

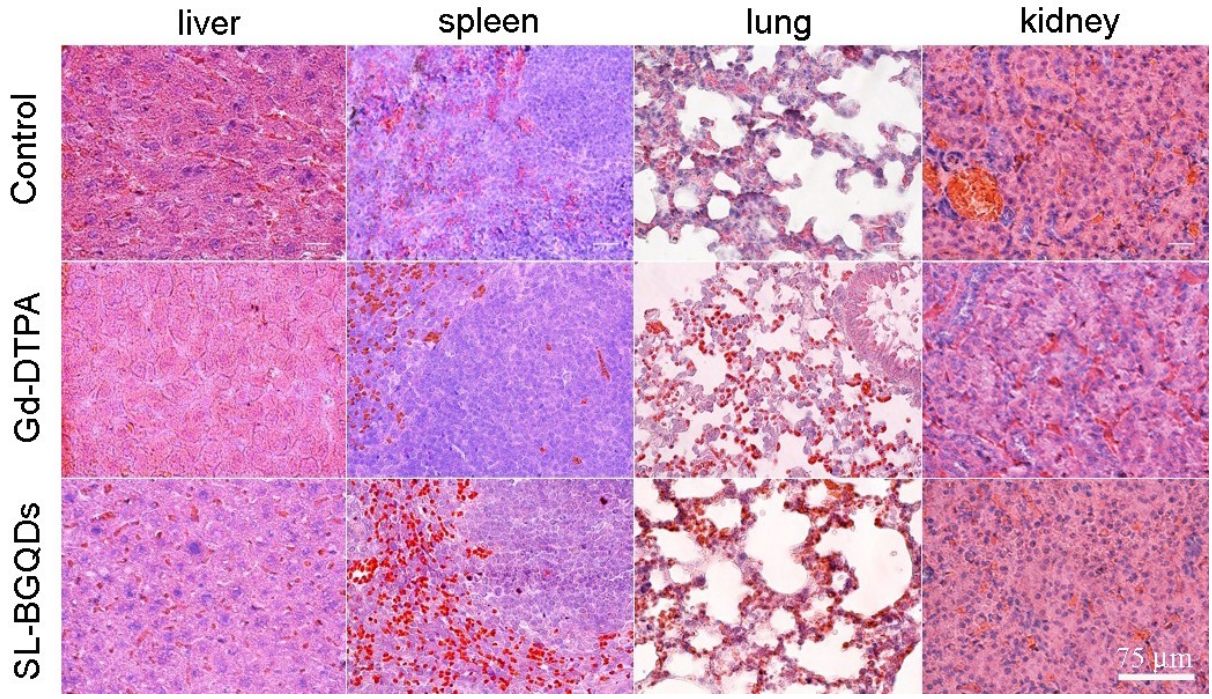

Figure S12. H&E staining of various organs harvested from the PBS- (control), Gd-DTPA-, and SL-BGQD-injected mice. The scale bar is 75 μm.

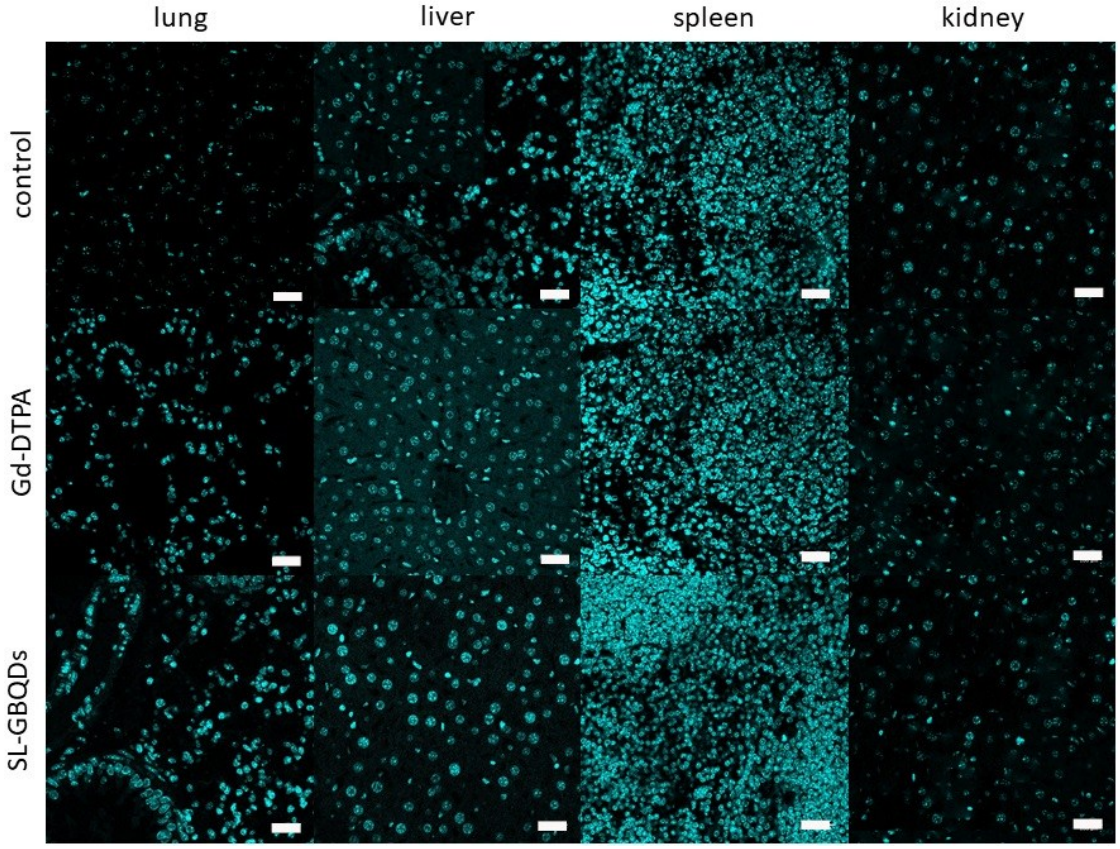

Figure S13. DAPI staining of various organ tissues obtained from mice treated with Gd-DTPA and SL-BGQD, with PBS-treated mice as control. The scale bar is 100 μm.

References

[1] H. Wang, J. Zhuang, D. Velado, Z. Wei, H. Matsui, S. Zhou, ACS Appl Mater Interfaces 2015, 7, 27703.
[2] D. Hulicova-Jurcakova, M. Seredych, G. Q. Lu, T. J. Bandosz, Advanced Functional Materials 2009, 19, 438.
[3] H. Wang, Y. Zhou, D. Wu, L. Liao, S. Zhao, H. Peng, Z. Liu, Small 2013, 9, 1316.
[4] S. Dey, A. Govindaraj, K. Biswas, C. N. R. Rao, Chemical Physics Letters 2014, 595–596, 203.
[5] Z. Zuo, Z. Jiang, A. Manthiram, Journal of Materials Chemistry A 2013, 1, 13476.
[6] H. Wang, J. Shen, Y. Li, Z. Wei, G. Cao, Z. Gai, K. Hong, P. Banerjee, S. Zhou, ACS Appl Mater Interfaces 2013, 5, 9446.